Title: Switching secretory pathway direction for organelle acquisition in plants

Authors: Takehiko Kanazawa[1,2], Hatsune Morinaka[3], Kazuo Ebine[1,2], Takashi L. Shimada[4], Sakiko Ishida[5], Naoki Minamino[1], Katsushi Yamaguchi[6], Shuji Shigenobu[6], Takayuki Kohchi[5], Akihiko Nakano[7], Takashi Ueda[1,2]*.

Affiliations:

[1]Division of Cellular Dynamics, National Institute for Basic Biology, Nishigonaka 38, Myodaiji, Okazaki, Aichi, 444-8585 Japan.

[2]The Department of Basic Biology, SOKENDAI (The Graduate University for Advanced Studies), Nishigonaka 38, Myodaiji, Okazaki, Aichi, 444-8585 Japan.

[3]Department of Biological Sciences, Graduate School of Sciences, The University of Tokyo, 7-3-1 Hongo, Bunkyo-ku, Tokyo 113-0033, Japan.

[4]Department of Applied Biological Chemistry, Graduate School of Horticulture, Chiba University, 648 Matsudo, Matsudo, Chiba, Japan.

[5]Graduate School of Biostudies, Kyoto University, Kitashirakawa-oiwake-cho, Sakyo-ku, Kyoto 606-8502, Japan.

[6]Functional Genomics Facility, National Institute for Basic Biology (NIBB), Okazaki, Aichi 444-8585, Japan.

[7]Live Cell Super-Resolution Imaging Research Team, RIKEN Center for Advanced Photonics, 2-1 Hirosawa, Wako, Saitama 351-0198, Japan.

*Correspondence to: tueda@nibb.ac.jp

Abstract:

Eukaryotic cells acquired novel organelles during evolution through mechanisms that remain largely obscure. The existence of the unique oil body compartment is a synapomorphy of liverworts that represents lineage-specific acquisition of this organelle during evolution, although its origin, biogenesis, and physiological function are yet unknown. We found that two Syntaxin 1 paralogs in the liverwort, *Marchantia polymorpha*, are distinctly targeted to forming cell plates and the oil body, suggesting these structures share some developmental similarity. Oil body formation is under the regulation of an ERF/AP2-type transcription factor and loss of the oil body increased *M. polymorpha* herbivory. These findings highlight a common strategy for the acquisition of organelles with distinct functions in plants, via periodical switching in secretion direction depending on cellular phase transition.

Main Text:

Eukaryotic cells originated from prokaryotes by expanding their endomembrane network during evolution, with the last eukaryotic common ancestor (LECA) likely possessing a complex set of organelles [1]. New membrane trafficking pathways were added to the LECA endomembrane network, some of which were secondarily lost in a lineage-specific manner, resulting in divergent and organism-specific membrane trafficking systems and organelle compositions of extant eukaryotes [2-4]. However, it remains mostly unknown how organelles were acquired during evolution. Also in the plant lineage, several organelles and organelle functions have been uniquely acquired during evolution. For example, the plant vacuole harbours a unique function that is not shared with the animal lysosome and the yeast vacuole: storage of proteins [5]. This vacuolar function is fulfilled through the plant-unique vacuolar trafficking system, which

45 comprises multiple vacuolar transport pathways involving plant-unique machinery components
46 acquired during plant evolution [6]. The cell plate, which is formed during the mitotic phase to
47 accomplish cytokinesis in land plants, is also a prominent example of plant-specific cellular
48 structures/organelles [7].
49 One of the basal-most land plant lineages, liverworts, also possess a unique organelle, the oil
50 body, existence of which is a synapomorphy of this lineage. The liverwort oil body contains
51 bioactive compounds such as sesquiterpenoids and cyclic bisbibenzyl compounds and is not
52 related to the oil body that stores neutral lipids in storage organs like seeds and fruits (i.e. lipid
53 body or oleosome). About 90% of liverwort species have this organelle; however, its origin,
54 biogenesis, and physiological function remain unclear with controversial origins proposed from
55 microscopic observations [8-11], although the first description of the liverwort oil body dates back
56 to 1834 [12]. Through the systematic analysis of SNARE proteins in the liverwort, *Marchantia*
57 *polymorpha* (hereafter referred to as Marchantia), we identified an oil body-resident protein,
58 MpSYP12B [13], which is a homolog of animal Syntaxin 1 that acts in the final step of exocytosis.
59 Functions of SYP1 members to which MpSYP12B belongs dramatically diversified during plant
60 evolution, suggesting expanded secretory trafficking systems in plants. Arabidopsis SYP1
61 consists of three subgroups, SYP11, SYP12, and SYP13. The SYP13 group mediates constitutive
62 secretion, whereas the other groups are involved in plant-specific higher ordered functions; for
63 example, KNOLLE (also known as SYP111) is specifically involved in membrane fusion at
64 forming cell plates, and PEN1 (also known as SYP121) is required for intact penetration
65 resistance against powdery mildew fungi and regulation of the ion channel activity [14-19]. For
66 more insight into the functional diversification of SYP1 members in Marchantia and the

67 mechanism of oil body biogenesis, we further characterized four SYP1 members in this organism
68 [13,20].
69
70 **MpSYP12A is important for cell plate formation**
71 Our phylogenetic analysis suggested that MpSYP1 members belong to two distinct subgroups:
72 the SYP13 group (MpSYP13A and 13B) and the SYP11/12 group (MpSYP12A and 12B) that
73 contains SYP11 and SYP12 groups in seed plants [21] (Fig. S1A). MpSYP12A, 13A and 13B were
74 ubiquitously expressed and localized to the plasma membrane (PM) in thallus tissues, whereas
75 MpSYP12B exhibited specific expression in a subpopulation of thallus cells (Fig S1B-E). Using
76 some ubiquitously expressed mCitrine-MpSYP1 protein fusion constructs driven by their own
77 regulatory elements, we detected specific localization of MpSYP12A at forming cell plates
78 associated with the phragmoplast that rapidly stained with FM4-64 (Figs. 1A-F, S1F, and S1G).
79 This localization suggested that MpSYP12A could be a functional counterpart of KNOLLE in
80 Arabidopsis, which was further verified genetically.
81 We tried to generate a complete Mp*syp12a* knockout mutant by genome editing (Fig. S1H) but
82 were not successful, probably because it is an essential gene. However, we succeeded in isolating
83 chimeric plants comprising mutated and wild-type cells, in which we frequently observed
84 enlarged cells with cell wall stabs, suggesting that MpSYP12A is required for cell plate
85 formation during cytokinesis similar to the function of KNOLLE (Fig. 1G). The *KNOLLE*
86 promoter is sufficient to target non-cytokinesis-specific SYP132 to forming cell plates [22].
87 Similarly, mCitrine-tagged MpSYP13A and 13B were localized to cell plates and the PM when
88 expressed under the Mp*SYP12A* promoter (Fig. 1H, I). Furthermore, a similar localization was
89 also observed when mCitrine-MpSYP13 was expressed by the Mp*CYCB1* promoter (Figs. 1J and

90 S1I), indicating that the cell cycle-dependent transcriptional regulation is also critical for cell
91 plate targeting of SYP1 proteins in Marchantia. We also found that clathrin light chain (CLC)
92 tagged with mCitrine localized to the PM and *trans*-Golgi network in non-dividing thallus cells,
93 as well as on forming cell plates in Marchantia as has been reported in other plants (Fig. S1J, K)
94 [23-25]. These results strongly suggested that fundamental mechanisms of cell plate formation were
95 conserved during land plant evolution.
96

97 **The oil body membrane shares common properties with the plasma membrane**

98 Distinct from the other MpSYP1 members, MpSYP12B exhibits specific expression in oil body
99 cells and localizes to the oil body membrane [13]. Oil body cells expressing a
100 $_{pro}$Mp*SYP12B:*2×YFP construct indicated that MpSYP12B distributed around meristematic
101 regions in young thalli, which was observed using light-sheet microscopy (Fig. 2A;
102 Supplementary movie S1). These results suggest that oil body formation occurs around
103 meristematic regions and into thalli during the growth of thallus tissues. mCitrine-MpSYP12B
104 expressed under its own regulatory elements localized to the oil body membrane with a faint
105 signal on the PM (Fig. 2B), which was also confirmed by immuno-EM analysis using an anti-
106 GFP antibody (Fig. 2C, D). We then tested whether organelle markers for the endoplasmic
107 reticulum (MpSEC20, MpUSE1A, MpSEC22, mRFP-HDEL, and GFP-HDEL), Golgi apparatus
108 (MpGOS11 and MpSFT1), *trans*-Golgi network (MpSYP6A and MpSYP4), and tonoplast
109 (MpSYP2 and MpVAMP71) were targeted to the oil body membrane, none of which were
110 detected (Figs. 2E and S2B, C). Using transmission electron microscopy, we found that clathrin-
111 coated vesicles formed from the oil body membrane, and emergence and disappearance of

112 clathrin-positive foci at the oil body membrane was also observed in transgenic plants expressing
113 Citrine-tagged MpCLC (Fig. 2G; Supplementary movie S2).
114 Given that clathrin-mediated endocytosis occurs at the PM and SYP1 members generally
115 function on the PM, the oil body membrane could share similar characteristics with the PM. This
116 hypothesis was supported by dual localization of the PM proteins, PM-type aquaporin MpPIP2
117 (Fig. 2H) and PM-resident SNARE MpSYP13A (Fig. 3A) driven by their own regulatory
118 elements. The plasma membrane-like nature of the oil body membrane and the existence of the
119 SYP1 member that is homologous to KNOLLE suggested that the oil body could be formed by
120 the fusion of secretory vesicles similar to the cell plate. Thus, the luminal space of the oil body
121 should be topologically equivalent to the extracellular space, which was tested by expressing a
122 general secretion marker sec-mRFP, which is composed of the signal peptide for ER
123 translocation and mRFP under the constitutive Mp*EF1α* promoter. In non-oil body cells, mRFP
124 fluorescence was detected only in the extracellular space (Fig. S2D). However, mRFP
125 accumulated in the oil body in addition to the extracellular space in oil body cells, demonstrating
126 equivalent topology between the lumen of the oil body and extracellular space (Fig. 2I). Unlike
127 MpSYP12A and KNOLLE, MpSYP12B loss of function did not result in a detectable
128 abnormality in oil body formation and transport of MpSYP13A or sec-mRFP (Fig. S3), probably
129 reflecting a functional redundancy between MpSYP12B and 13A similar to the partial functional
130 redundancy of KNOLLE and SYP132 [26].
131
132 **The oil body is formed by directional switching of the secretory pathway**
133 Distinct from MpSYP13A with the dual localization to the plasma and oil body membranes, the
134 close homolog MpSYP13B was only localized to the PM in oil body cells (Fig. 3A, B).

135 Surprisingly, both of these proteins were targeted predominantly to the oil body membrane when
136 expressed under the regulation of the Mp*SYP12B* promoter (Fig. 3C, D). This effect was not
137 restricted to SYP1 homologs; the PM-resident protein MpPIP2 and a general secretion cargo sec-
138 mRFP were also targeted almost exclusively to the oil body when driven by the Mp*SYP12B*
139 promoter (Fig. 3E, F). These results indicated that the secretory pathway is redirected inward and
140 vesicles fuse with each other to form the oil body during the phase in which the Mp*SYP12B*
141 promoter is active. In contrast, when Mp*SYP13B* promoter is active, the secretory pathway is
142 directed to the PM and extracellular space, which was further confirmed by accumulation of sec-
143 mRFP predominantly in the extracellular space when the construct was driven by the Mp*SYP13B*
144 promoter (Fig. 3G). Other organelle markers did not change their localization even when
145 expressed under the Mp*SYP12B* promoter (Fig. S2B, C). These results indicated that the
146 switching of directions of the secretory pathway in oil body cells is regulated at the transcription
147 level. The switching of secretory directions should take place periodically and repeatedly
148 through oil body cell development, because we never observed oil body membrane localization
149 for MpSYP13B at any developmental stages of oil body cells (Fig. 4A-C), and increase in the
150 size of the oil body cell along with the increase in the oil body size was observed (Fig. 4D).
151 Based on these findings, we propose the "oil body cycle hypothesis", which states that
152 Marchantia oil body cells cycle between two distinct cellular phases: the "PM phase" in which
153 the secretory pathway is oriented to the PM and extracellular space, and the "oil body phase"
154 when the secretory pathway is oriented to the oil body, with the phase transition under the
155 regulation of a transcriptional regulatory system (Fig. 4E, F).

156

157

158 **MpERF13 transcription factor regulates oil body formation**

159 To investigate the regulatory system of oil body formation and oil body cycle, we screened
160 mutants defective in oil body formation (Fig. S4A). From 48,825 T-DNA insertion lines, we
161 identified a mutant (Mp*erf13*^{GOF}) with an increased number of oil bodies. The mutant gemmae
162 contained 334.4 ± 85.6 oil bodies (mean ± SD), whereas wild-type gemmae possessed 51.9 ± 8.7
163 oil bodies under our experimental conditions (Fig. 5A-E). The T-DNA was inserted 2674-bp
164 upstream of the start codon of Mapoly0060s0052.1 (Mp*ERF13*), which encodes a putative
165 ERF/AP2 transcription factor in the subgroup containing DREB1A and TINY in Arabidopsis
166 (Fig. S4B). Moreover, Mp*ERF13* and Mp*SYP12B* transcripts accumulated in this mutant
167 compared to wild type as detected by RNA-sequencing (RNA-Seq) and quantitative RT-PCR
168 analyses (Fig. S5B). We then generated knockout mutants in which the Mp*ERF13* gene was
169 deleted by genome editing (Fig. S4C). Two independent mutants (Mp*erf13-1*^{ge} and Mp*erf13-2*^{ge})
170 exhibited no detectable abnormalities in thallus development and reproductive growth; however,
171 these mutants completely lacked oil bodies in the gemma and thallus tissues (Figs. 5C-E and
172 S4F, G). These phenotypes of gain- and loss-of-function mutations suggested that MpERF13 is a
173 major transcription factor regulating oil body formation. Consistently, the Mp*ERF13* promoter
174 was highly active in oil body cells (Fig. 5F).

175 As MpERF13 is homologous to ERF/AP2 transcription factors, this protein was expected to be
176 involved in the transcriptional regulation of oil body formation and/or the oil body cycle. To
177 identify genes downstream of MpERF13, we analyzed transcriptomes in Tak-1 (wild type) and
178 Mp*erf13*^{GOF} and Mp*erf13-1*^{ge} mutant lines by RNA-Seq. Through the comparison between the
179 three groups using an ANOVA-like test, we identified 136 differentially-expressed genes
180 (DEGs) other than Mp*ERF13* whose expression was higher than two $\log_2$-fold change (FC) in

181 Mp*erf13*^{GOF} compared with Tak-1, and lower than -2 $\log_2$FC in Mp*erf13-1*^{ge} than Tak-1 (FDR <
182 0.01) (Supplementary Table S1). To verify the RNA-Seq result, we also performed the
183 quantitative RT-PCR analysis for selected 11 DEGs including Mp*ERF13* and Mp*SYP12B*, which
184 confirmed that all of these DEGs were highly expressed in Mp*erf13*^{GOF}, but their expression was
185 significantly lower or not detectable in Mp*erf13-1*^{ge} and Mp*erf13-2*^{ge} compared with Tak-1 (Fig
186 S5). These data strongly suggested that these 136 genes function downstream of Mp*ERF13* in oil
187 body cells, which was further verified for the two genes Mapoly0083s0014.1 and MpMYB02
188 (Mapoly0006s0226). Mapoly0083s0014.1 was positively regulated by MpERF13 and encodes a
189 member of the G subfamily of ABC transporters [20], which we named MpABCG1. Although
190 ABCG members are generally targeted to the PM and mediate efflux of secondary metabolites
191 from intracellular to extracellular spaces [27,28], mCitrine-MpABCG1 was targeted to the oil body
192 membrane when expressed under its own regulatory elements (Fig. 5G); however, this protein
193 was targeted to the PM in non-oil body cells when expressed under the Mp*SYP13B* promoter
194 (Fig. 5H). MpMYB02, whose expression was also positively regulated by MpERF13, is reported
195 to be a transcription factor responsible for the production of marchantin A and its derivatives that
196 accumulate in oil bodies [11,29]. Mp*ABCG1* and Mp*MYB02* are specifically expressed in oil body
197 cells and when sec-mRFP was driven by the promoters of these genes, it was specifically
198 targeted to the lumen of oil bodies. These results indicated that MpABCG1 and MpMYB02,
199 presumably together with other DEGs we identified, act during oil body formation downstream
200 of MpERF13.
201 Lastly, we asked why liverworts possess oil bodies. Using fresh and alcohol-washed liverworts,
202 the oil body was proposed to be an effective chemical protection from herbivores [30], although its
203 true function remains unknown because alcohol can wash out substances as well as oil body

204 constituents. We fed starved *Armadillidium vulgare* (pill bug) with wild-type liverwort and
205 genetically established mutants that contain extra or no oil bodies. Thalli of Tak-1 and
206 Mp*erf13*^{GOF} remained almost intact after 24 h of herbivory, while the areas of Mp*erf13-1*^{ge} and
207 Mp*erf13-2*^{ge} thalli were significantly reduced after herbivory (Figs. 6 and S6). This result
208 demonstrated that the oil body is effective in protecting liverworts from herbivores.
209
210 We demonstrate that plants have acquired at least two organelles, the cell plate and oil body,
211 through a common evolutionary pathway of redirecting secretory patterns from an outward to an
212 inward direction in cells. The functions of these organelles are totally different but they share
213 several important traits that include specific SYP11/12 members that reside at their membranes,
214 clathrin-coated vesicles generated from the plasma and internal membranes, and both the cell
215 plate and oil body are formed by reorientation of secretory pathways. In both cases, orientation
216 of the secretory pathway is switched in response to transitioning cellular states, during the cell
217 cycle for cell plate formation and the oil body cycle for oil body formation. Orientation of the
218 plant secretory pathway is also modulated during plant-microbe interactions; symbiotic
219 arbuscular mycorrhizal fungi redirects the plant secretory pathway to form the arbuscule in host
220 plant cells that acts as an interface for sugar and mineral exchange [31,32]. Thus, redirection of the
221 secretory pathway is a common strategy for plants to acquire novel organelles/cellular structures
222 that had resulted in maximizing fitness for land plants during evolution. The liverwort oil body is
223 a nice system to evaluate how novel organelles have been acquired during evolution, and the
224 knowledge obtained from this study is useful for engineering new organelles/cellular structures
225 in plants to maximize plant cellular functions and provides a powerful methodology for future
226 organelle technology.

227 **Acknowledgments:** We thank Dr. Ikuko Hara-Nishimura (Konan University), Dr. Kimitsune
228 Ishizaki (Kobe University), Dr. Ryuichi Nishihama (Kyoto University), and Dr. Shigeo S.
229 Sugano for sharing vectors and plant materials, Ms. Miwako Matsumoto, Ms. Asaka Akita, and
230 Functional Genomics Facility (NIBB) for technical assistance in RNA-Seq experiments, and Dr.
231 Ken Naito (National Agriculture and Food Research Organization) for instruction for RNA-Seq
232 data analysis. We thank Dr. John L. Bowman (Monash University) and Dr. Facundo Romani
233 (Universidad Nacional del Litoral) for helpful discussion. We also thank Dr. Teruyuki Niimi
234 (NIBB) and Dr. Takahisa Miyatake (Okayama University) for identification of the species of pill
235 bug used in this study. The support of plant cultivation rooms was provided by the Model Plant
236 Research Facility of NIBB.

237

238 **Funding:** This work was financially supported by Grants-in-Aid for Scientific Research from the
239 Ministry of Education, Culture, Sports, Science, and Technology of Japan (to T.U., 19H05670,
240 19H05675, and 18H02470, and T.Ka., 18K14738).

241

242 **Author contributions:** T.Ka. performed the majority of the experiments, H.M. performed the
243 experiment presented in Fig. 1A-G, K.E. and T.L.S. provided essential ideas for experiments
244 using sec-mRFP targeting and oil body detection, respectively, S.I. generated the Mp*syp12b-1*
245 mutant, K.Y. and S.S. designed the RNA-seq experiment, N.M. examined the effect of Mp*erf13*
246 mutations on reproductive growth, T.Ka. and T.U. wrote the manuscript, and T.Ko., A.N., and
247 T.U. supervised the study.

248

249 **Competing interests:** Authors declare no competing interests.

250

251 **Data and materials availability:** All reads of RNA-Seq are available through the Sequence

252 Read Archive (SRA) under the accession number DRA009193.

253

254 **References:**

255 1 Koumandou, V. L. *et al.* Molecular paleontology and complexity in the last eukaryotic
256 common ancestor. *Critical reviews in biochemistry and molecular biology* **48**, 373-396,
257 doi:10.3109/10409238.2013.821444 (2013).

258 2 Kanazawa, T. & Ueda, T. Exocytic trafficking pathways in plants: why and how they are
259 redirected. *The New phytologist* **215**, 952-957, doi:10.1111/nph.14613 (2017).

260 3 Klinger, C. M., Nisbet, R. E., Ouologuem, D. T., Roos, D. S. & Dacks, J. B. Cryptic
261 organelle homology in apicomplexan parasites: insights from evolutionary cell biology.
262 *Current opinion in microbiology* **16**, 424-431, doi:10.1016/j.mib.2013.07.015 (2013).

263 4 L'Hernault, S. W. Spermatogenesis. *WormBook : the online review of C. elegans biology*,
264 1-14, doi:10.1895/wormbook.1.85.1 (2006).

265 5 Shimada, T., Takagi, J., Ichino, T., Shirakawa, M. & Hara-Nishimura, I. Plant Vacuoles.
266 *Annual review of plant biology* **69**, 123-145, doi:10.1146/annurev-arplant-042817-
267 040508 (2018).

268 6 Minamino, N. & Ueda, T. RAB GTPases and their effectors in plant endosomal transport.
269 *Current opinion in plant biology* **52**, 61-68, doi:10.1016/j.pbi.2019.07.007 (2019).

270 7 Müller, S. & Jürgens, G. Plant cytokinesis-No ring, no constriction but centrifugal
271 construction of the partitioning membrane. *Seminars in cell & developmental biology* **53**,
272 10-18, doi:10.1016/j.semcdb.2015.10.037 (2016).

273 8 Asakawa, Y., Ludwiczuk, A. & Nagashima, F. Phytochemical and biological studies of
274 bryophytes. *Phytochemistry* **91**, 52-80, doi:10.1016/j.phytochem.2012.04.012 (2013).

275 9 He, X. L., Sun, Y. & Zhu, R. L. The Oil Bodies of Liverworts: Unique and Important
276 Organelles in Land Plants. *Critical Reviews in Plant Sciences* **32**, 293-302,
277 doi:10.1080/07352689.2013.765765 (2013).

278 10 Suire, C. A comparative, transmission-electron microscopic study on the formation of oil-
279 bodies in liverworts. *J Hattori Bot Lab*, 209-232 (2000).

280 11 Tanaka, M. *et al.* Direct evidence of specific localization of sesquiterpenes and
281 marchantin A in oil body cells of *Marchantia polymorpha* L. *Phytochemistry* **130**, 77-84,
282 doi:10.1016/j.phytochem.2016.06.008 (2016).

283 12 Hübener, J. W. P. Hepaticologia germanica, oder Beschreibung der Deutschen
284 lebermoose. *Schwan & Götz'sche Hofbuchlandlung, Mannheim* (1834).

285 13 Kanazawa, T. *et al.* SNARE Molecules in *Marchantia polymorpha*: Unique and
286 Conserved Features of the Membrane Fusion Machinery. *Plant & cell physiology* **57**,
287 307-324, doi:10.1093/pcp/pcv076 (2016).

288 14 Assaad, F. F. *et al.* The PEN1 syntaxin defines a novel cellular compartment upon fungal
289 attack and is required for the timely assembly of papillae. *Mol Biol Cell* **15**, 5118-5129,
290 doi:10.1091/mbc.E04-02-0140 (2004).

291 15 Collins, N. C. *et al.* SNARE-protein-mediated disease resistance at the plant cell wall.
292 *Nature* **425**, 973-977, doi:10.1038/nature02076 (2003).

293 16 Enami, K. *et al.* Differential expression control and polarized distribution of plasma
294 membrane-resident SYP1 SNAREs in *Arabidopsis thaliana*. *Plant & cell physiology* **50**,
295 280-289, doi:10.1093/pcp/pcn197 (2009).

296 17 Grefen, C. *et al.* A vesicle-trafficking protein commandeers Kv channel voltage sensors
297 for voltage-dependent secretion. *Nature plants* **1**, 15108, doi:10.1038/nplants.2015.108
298 (2015).

299 18 Lauber, M. H. *et al.* The Arabidopsis KNOLLE protein is a cytokinesis-specific syntaxin.
300 *Journal of Cell Biology* **139**, 1485-1493, doi:DOI 10.1083/jcb.139.6.1485 (1997).

301 19 Lukowitz, W., Mayer, U. & Jurgens, G. Cytokinesis in the Arabidopsis embryo involves
302 the syntaxin-related KNOLLE gene product. *Cell* **84**, 61-71, doi:Doi 10.1016/S0092-
303 8674(00)80993-9 (1996).

304 20 Bowman, J. L. *et al.* Insights into Land Plant Evolution Garnered from the *Marchantia*
305 *polymorpha* Genome. *Cell* **171**, 287-304 e215, doi:10.1016/j.cell.2017.09.030 (2017).

306 21 Slane, D., Reichardt, I., El Kasmi, F., Bayer, M. & Jurgens, G. Evolutionarily diverse
307 SYP1 Qa-SNAREs jointly sustain pollen tube growth in Arabidopsis. *The Plant journal :*
308 *for cell and molecular biology* **92**, 375-385, doi:10.1111/tpj.13659 (2017).

309 22 Reichardt, I. *et al.* Mechanisms of Functional Specificity Among Plasma-Membrane
310 Syntaxins in Arabidopsis. *Traffic* **12**, 1269-1280, doi:10.1111/j.1600-0854.2011.01222.x
311 (2011).

312 23 Ito, E. *et al.* Dynamic behavior of clathrin in Arabidopsis thaliana unveiled by live
313 imaging. *The Plant journal : for cell and molecular biology* **69**, 204-216,
314 doi:10.1111/j.1365-313X.2011.04782.x (2012).

315 24 Otegui, M. S., Mastronarde, D. N., Kang, B. H., Bednarek, S. Y. & Staehelin, L. A.
316 Three-dimensional analysis of syncytial-type cell plates during endosperm cellularization

317 visualized by high resolution electron tomography. *The Plant cell* **13**, 2033-2051,
318 doi:10.1105/tpc.010150 (2001).

319 25 Samuels, A. L., Giddings, T. H., Jr. & Staehelin, L. A. Cytokinesis in tobacco BY-2 and
320 root tip cells: a new model of cell plate formation in higher plants. *The Journal of cell*
321 *biology* **130**, 1345-1357, doi:10.1083/jcb.130.6.1345 (1995).

322 26 Park, M. *et al.* Concerted Action of Evolutionarily Ancient and Novel SNARE
323 Complexes in Flowering-Plant Cytokinesis. *Developmental cell* **44**, 500-511 e504,
324 doi:10.1016/j.devcel.2017.12.027 (2018).

325 27 Adebesin, F. *et al.* Emission of volatile organic compounds from petunia flowers is
326 facilitated by an ABC transporter. *Science* **356**, 1386-1388, doi:10.1126/science.aan0826
327 (2017).

328 28 Kang, J. *et al.* Plant ABC Transporters. *The arabidopsis book* **9**, e0153,
329 doi:10.1199/tab.0153 (2011).

330 29 Kubo, H. *et al.* Biosynthesis of riccionidins and marchantins is regulated by R2R3-MYB
331 transcription factors in *Marchantia polymorpha*. *Journal of plant research* **131**, 849-864,
332 doi:10.1007/s10265-018-1044-7 (2018).

333 30 Stahl, E. Pflanzen und Schnecken. *Jena. Z. Med. Naturwiss* **22**, 557 - 684 (1888).

334 31 Ivanov, S. & Harrison, M. J. A set of fluorescent protein-based markers expressed from
335 constitutive and arbuscular mycorrhiza-inducible promoters to label organelles,
336 membranes and cytoskeletal elements in *Medicago truncatula*. *The Plant journal : for*
337 *cell and molecular biology* **80**, 1151-1163, doi:10.1111/tpj.12706 (2014).

338 32 Pumplin, N., Zhang, X., Noar, R. D. & Harrison, M. J. Polar localization of a symbiosis-
339 specific phosphate transporter is mediated by a transient reorientation of secretion.
340 *Proceedings of the National Academy of Sciences of the United States of America* **109**,
341 E665-672, doi:10.1073/pnas.1110215109 (2012).

342

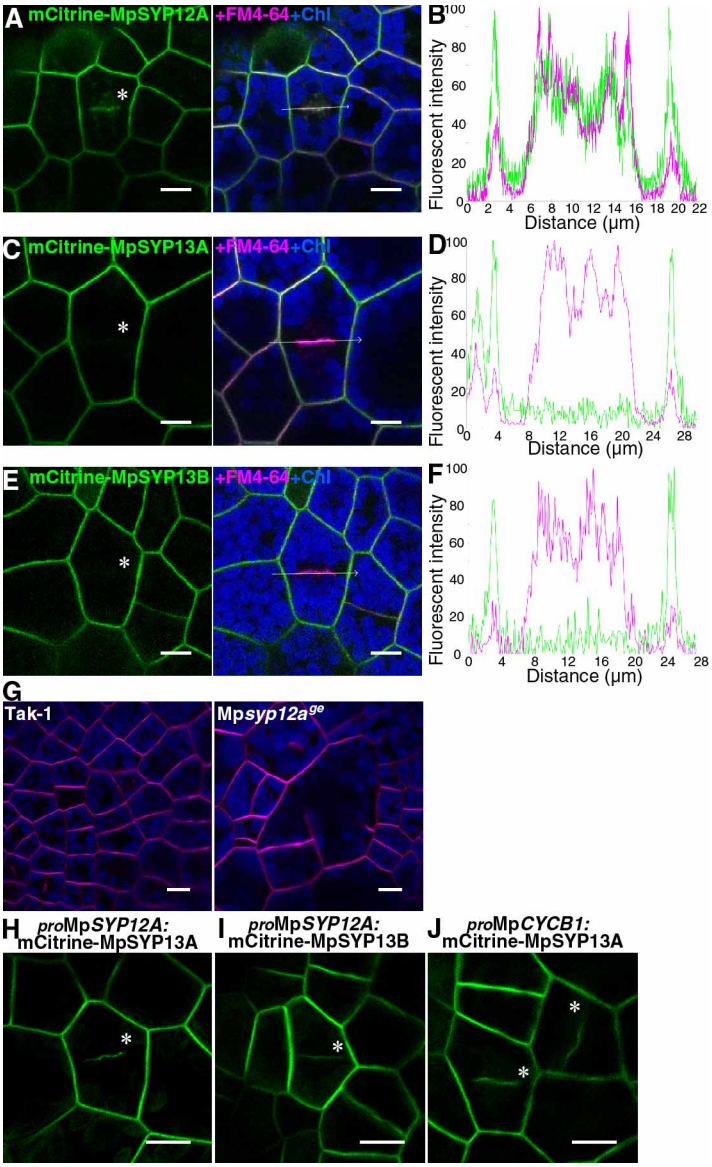

Fig. 1. MpSYP12A is important for cell plate formation in *M. polymorpha* thallus cells. (A, C, and E) Marchantia thallus cells expressing mCitrine-MpSYP12A (A), mCitrine-MpSYP13A (C), and mCitrine-MpSYP13B (E) stained with FM4-64. (B, D, and F) Line graphs showing relative fluorescence intensities from mCitrine and FM4-64 along the white arrows in panels A (B), C (D), and E (F). (G) Thallus cells of Tak-1 (left) and a putative knock-out mutant (right) stained with FM4-64. (H and I) Dividing thallus cells expressing mCitrine-MpSYP13A (H) or mCitrine-MpSYP13B (I) driven by the Mp*SYP12A* promoter. (J) Dividing thallus cells

350 expressing mCitrine-MpSYP13A under the regulation of the Mp*CYCB1* promoter. Asterisks
351 indicate forming cell plates. Green, magenta, and blue pseudo-colors indicate fluorescence from
352 mCitrine, FM4-64, and chlorophyll, respectively. Bars = 10 μm.
353

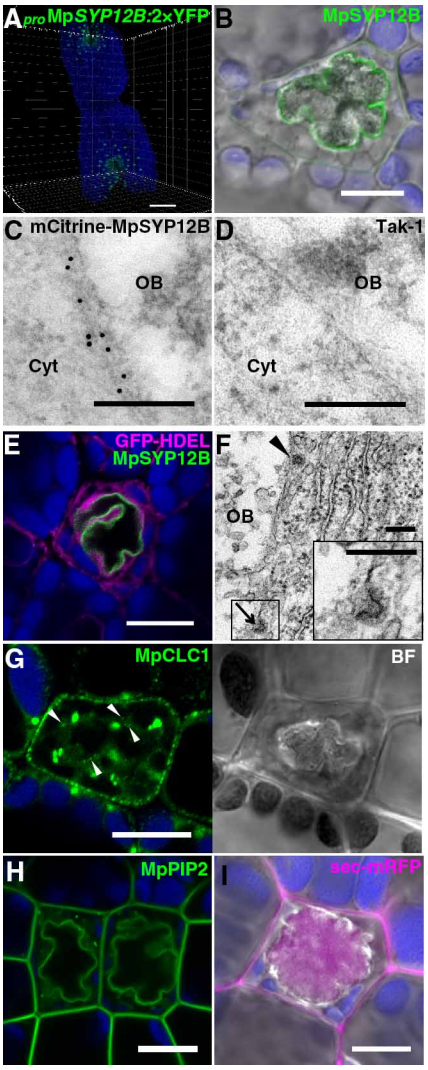

Fig. 2. The oil body membrane shares common properties with the plasma membrane. (A) A five-day-old thallus expressing 2×Citrine (YFP) under the regulation of the Mp*SYP12B* promoter observed with a light sheet microscope. (B) An oil body cell expressing mCitrine-MpSYP12B under its own regulatory elements. The bright field image was merged. (C and D) Immunoelectron micrographs of oil body cells in thalli of Tak-1 with (C) or without (D) mCitrine-MpSYP12B expression. Cyt, cytosol, and OB, oil body. (E) An oil body cell expressing GFP-HDEL (magenta) and mCitrine-MpSYP12B (green). (F) An electron micrograph of the oil body cell. The arrowhead and arrow indicate a clathrin-coated vesicle and a clathrin-coated pit, respectively. The magnified image of the boxed region is shown in the inset.

363 (G) An oil body cell expressing MpCLC1-Citrine. Arrowheads indicate clathrin-coated
364 vesicles/pits on the oil body membrane. BF, bright field image. (H) Oil body cells expressing
365 mCitrine-MpPIP2 under its own regulatory elements. (I) An oil body cell expressing sec-mRFP
366 driven by the Mp*EF1α* promoter. The bright field image was merged. The blue pseudo-color
367 indicates chlorophyll autofluorescence. Bars = 500 μm in (A), 10 μm in (B), (E), and (G - I), and
368 200 nm in (C), (D), and (F).
369

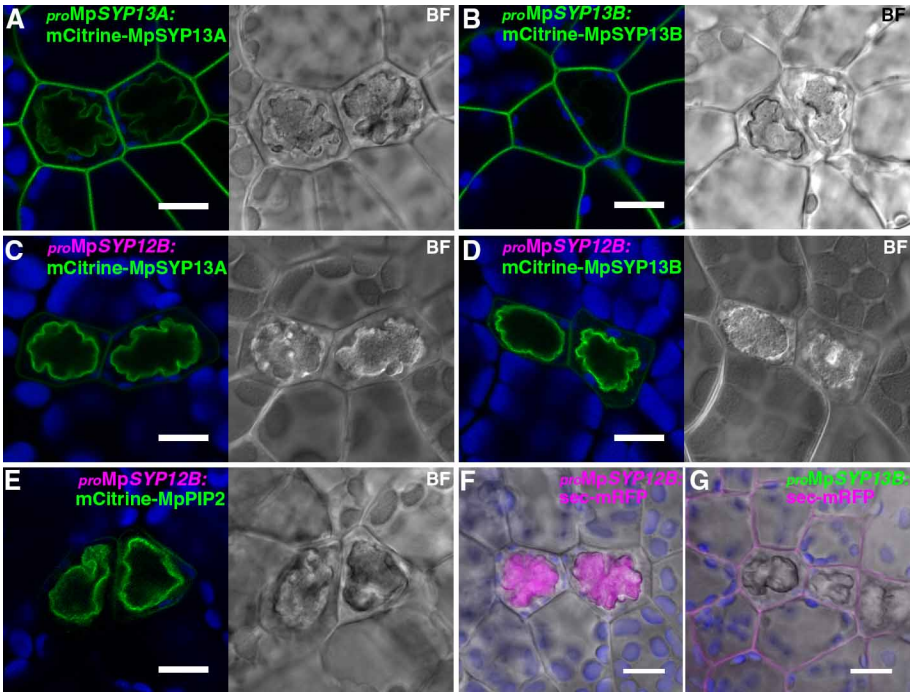

Fig. 3. The oil body is formed by directional switching of the secretory pathway (A and B) Thallus cells including oil body cells expressing mCitrine-MpSYP13A (A) or mCitrine-MpSYP13B (B) under their own regulatory elements. (C - E) Thallus cells including oil body cells expressing mCitrine-MpSYP13A (C), mCitrine-MpSYP13B (D), or mCitrine-MpPIP2 (E) under the Mp*SYP12B* promoter. BF, bright field images. (F and G) Thallus cells including oil body cells expressing sec-mRFP under the Mp*SYP12B* promoter (F) or the Mp*SYP13B* promoter (G). Bright field images are merged. Bars = 10 μm.

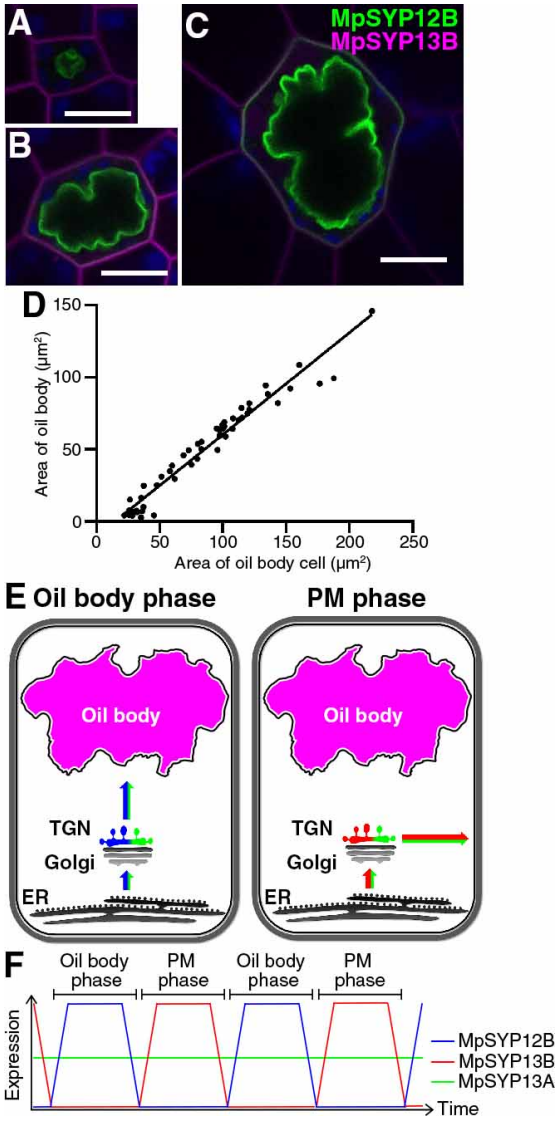

Fig. 4. The oil body cycle hypothesis (A - C) Oil body cells at distinct developmental stages expressing mCitrine-MpSYP12B and mRFP-MpSYP13B. Green, magenta, and blue pseudo-colors indicate mCitrine, mRFP, and autofluorescence from chlorophyll, respectively. Bars = 10 μm. (D) A scatter diagram of the areas of oil body cells on the X axis and the areas of oil bodies on the Y axis. $R^2 = 0.9547$. (E and F) Schemes of the oil body cycle hypothesis. Newly synthesized PM proteins and secreted cargos are targeted to the oil body membrane in the oil body phase, and then to the PM and extracellular space during the PM phase (E). Expression levels of MpSYP12B and MpSYP13B periodically oscillate depending on the cell phases;

387 whereas, MpSYP13A is constitutively expressed, resulting in dual localization at the oil body

388 membrane and the PM (F).

389

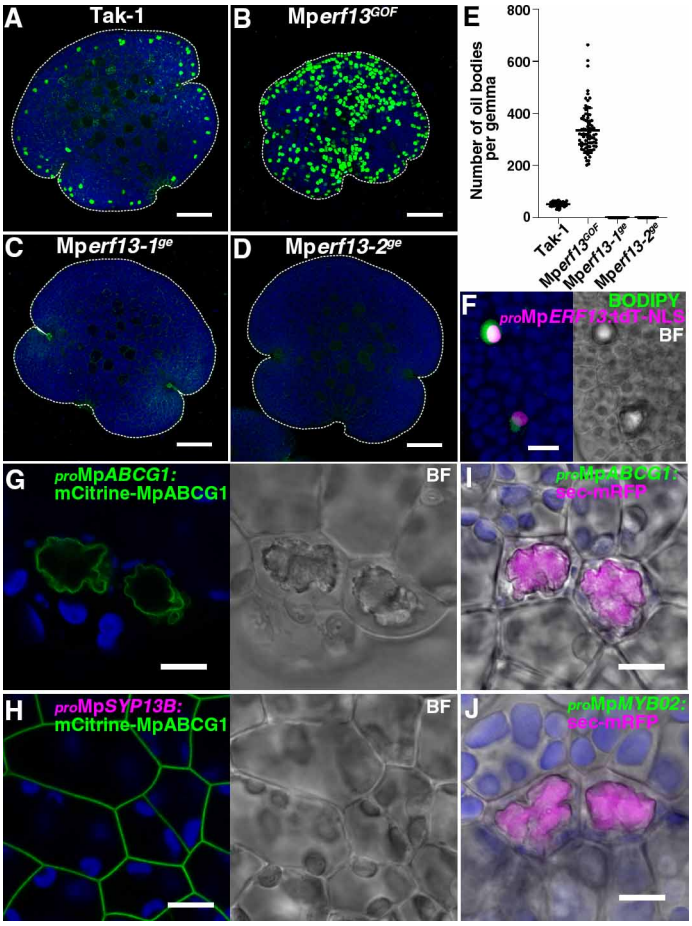

Fig. 5. MpERF13 transcription factor regulates oil body formation. (A - D) Maximum - intensity projection images of BODIPY-stained gemmae of Tak-1 (A), Mp*erf13*^{GOF} (B), Mp*erf13-1*^{ge} (C), and Mp*erf13-2*^{ge} (D). (E) The number of oil bodies visualized by BODIPY-staining in gemmae. Bars indicate means ± SD. Statistical analyses between Tak-1 and each genotype were conducted using a two-tailed Welch's *t*-test. Sample numbers were 57 gemmae for Tak-1, 78 for Mp*erf13*^{GOF}, 61 for Mp*erf13-1*^{ge}, and 75 for Mp*erf13-2*^{ge}; and *p*-values are 1.19×10^{-43} for Mp*erf13*^{GOF}, 1.44×10^{-45} for Mp*erf13-1*^{ge}, and 1.44×10^{-45} for Mp*erf13-2*^{ge}. (F) A maximum intensity projection image of oil body and non-oil body cells in a gemma expressing tandemTomato (tdT)-NLS driven by the Mp*ERF13* promoter. (G and H) Thallus cells including oil body cells expressing mCitrine-MpABCG1 under its own regulatory elements (G) and the Mp*SYP13B* promoter (H). BF, bright field images. (I and J) Thallus cells expressing sec-mRFP

401 under the Mp*ABCG1* (I) and the Mp*MYB02* (J) promoters. Bright field images are merged.

402 Green, magenta, and blue pseudo-colors indicate fluorescence from BODIPY or mCitrine, tdT or

403 mRFP, and chlorophyll, respectively. Bars = 100 µm in (A - D) and 10 µm in (F - J).

404

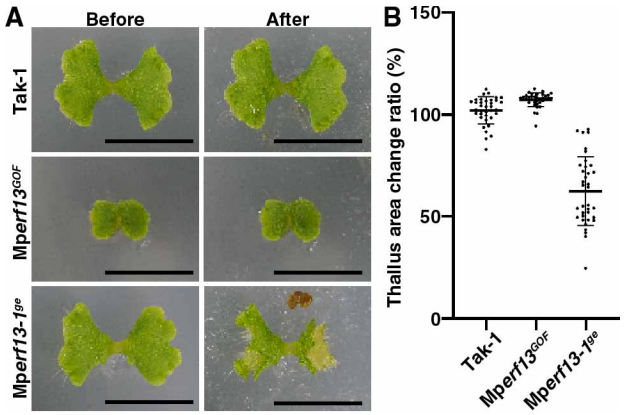

Fig. 6 (A) Ten-day-old thalli in indicated genotypes (Before) they were fed to starved pill bugs or 24 h after feeding (After). (B) Quantification of fluorescence signals images in panel (A). Ratios of thallus areas of "After" to "Before" pill bug feeding were calculated to indicate thallus area change ratios (n = 36 thalli for each genotype). Bars indicate means ± SD. Statistical analyses between Tak-1 and each genotype were conducted by two-tailed Welch's *t*-test. The *p*-values were 5.21×10^{-4} for Mp*erf13*^{GOF} and 1.05×10^{-16} for Mp*erf13-1*^{ge}. Bars = 1 cm.

Supplementary Information for

Switching secretory pathway direction for organelle acquisition in plants

Takehiko Kanazawa, Hatsune Morinaka, Kazuo Ebine, Takashi L. Shimada, Sakiko Ishida, Naoki Minamino, Katsushi Yamaguchi, Shuji Shigenobu, Takayuki Kohchi, Akihiko Nakano, Takashi Ueda.

Correspondence to: tueda@nibb.ac.jp

This PDF file includes:

Materials and Methods
Supplementary Text
Figs. S1 to S6
Captions for Tables S1 & S2
Captions for Movies S1 & S2
References 33-54

Other Supplementary Materials for this manuscript include the following:

Movies S1 & S2
Table S1 & S2

437 **Materials and Methods**

438 Phylogenetic Analyses

439 Phylogenetic analyses were performed as previously described in Bowman *et al*, 2017 [20]
440 with minor modification. Previously published datasets in Kanazawa *et al*., 2016 and Bowman *et*
441 *al*., 2017, were used for phylogenetic analyses of SYP1 and ERF/AP2 members, respectively
442 [13,20]. Multiple sequence alignments were performed using the MUSCLE program version 3.8.31
443 [33,34] with the default parameter. The alignment gaps were removed by Gblocks program version
444 0.91b [35,36] or manually. The maximum likelihood phylogenetic analyses were performed using
445 PhyML 3.0 [37] under the LG model. Bootstrap analyses were performed by resampling 1000 sets.
446

447 Vector Construction

448 Open reading frames (ORFs) and genomic sequences of Marchantia genes were amplified
449 by polymerase chain reaction (PCR) from cDNA and genomic DNA prepared from the accession
450 Tak-1, and the amplified products were subcloned into pENTR/D-TOPO (ThermoFisher,
451 Waltham, USA) according to the manufacturer's instructions. The primer sequences and sizes of
452 amplified products are listed in Supplementary Table S2. For construction of pENTR
453 $_{pro}$Mp*ERF13*, the 5′ sequence (promoter + 5′ UTR) was amplified and subcloned into pENTR/D-
454 TOPO. The resultant sequence was introduced into pMpGWB316 [38] using the Gateway LR
455 Clonase™ II Enzyme Mix (ThermoFisher) according to the manufacturer's instructions. For
456 construction of pENTR genomic mGFP-MpSYP12A and mRFP-MpSYP13B constructs, the
457 cDNA for mGFP and mRFP were inserted into *Sma*I and *Bam*HI sites in the pENTR genomic
458 XFP(*Sma*I)-MpSYP12A and pENTR genomic XFP(*Bam*HI)-MpSYP13B, which were
459 previously prepared [13] using the In-Fusion HD Cloning System (Clontech, Shiga, Japan). For
460 construction of pENTR genomic mCitrine-MpPIP2, pENTR genomic mCitrine-MpSYP4,
461 pENTR genomic mCitrine-MpSEC22, and pENTR genomic mCitrine-MpABCG1, genomic
462 sequences of the protein-coding regions and 3′ flanking sequences were amplified with a *Sma*I
463 site at the 5′ end and subcloned into the pENTR vector. The 5′ sequences (promoter + 5′ UTR)
464 and cDNA of mCitrine were amplified and inserted into *Not*I and *Sma*I sites, respectively, of the
465 resultant pENTR vectors using the In-Fusion HD Cloning System. The resultant chimeric genes
466 were then introduced into pMpGWB301 [38] using the Gateway LR Clonase™ II Enzyme Mix.
467 For construction of pENTR $_{pro}$Mp*SYP12B:mCitrine*, the $_{pro}$Mp*SYP12B:mCitrine* sequence was

468 amplified from the pENTR genomic mCitrine-MpSYP12B vector, and subcloned into
469 pENTR/D-TOPO. The resultant sequence was introduced into pMpGWB307 [38] using the
470 Gateway LR Clonase™ II Enzyme Mix to create the pMpGWB307 $_{pro}$Mp*SYP12B:2×YFP*
471 construct. For construction of pENTR genomic MpCLC1-mCitrine, genomic sequence
472 comprising the 5′ flanking (promoter + 5′ UTR) and protein-coding sequences were amplified
473 with a *Sma*I site at the 3′ end and subcloned into the pENTR vector. The 3′ flanking sequence
474 including 3′ UTR and cDNA for mCitrine were amplified and inserted into *Asc*I and *Sma*I sites,
475 respectively, of the resultant pENTR vectors using the In-Fusion HD Cloning System. The
476 resultant chimeric genes were then introduced into pMpGWB301 [38] using the Gateway LR
477 Clonase™ II Enzyme Mix. For construction of pENTR sec-mRFP, sequences for the signal
478 peptide and mRFP were independently amplified by PCR, and the sequence of sec-mRFP was
479 then amplified by PCR using the mixture of the amplified products as templates. The amplified
480 products were subcloned into pENTR/D-TOPO. For the construction of pENTR mRFP-HDEL,
481 the sequence of SP-mRFP-HDEL was amplified by PCR using pENTR sec-mRFP as template,
482 and subcloned into pENTR/D-TOPO. For construction of pENTR $_{pro}$Mp*SYP12B:*sec-mRFP,
483 pENTR $_{pro}$Mp*SYP13B:*sec-mRFP, pENTR $_{pro}$Mp*ABCG1:*sec-mRFP, and pENTR
484 $_{pro}$Mp*MYB02:*sec-mRFP, the 5′ sequences (promoter + 5′ UTR) were amplified and were
485 inserted into *Not*I sites of the pENTR sec-mRFP vector using the In-Fusion HD Cloning System.
486 The resultant sequences were then introduced into pMpGWB301 [38] using the Gateway LR
487 Clonase™ II Enzyme Mix. To construct pMpGWB301-derived Gateway vectors (Fig. S2A), the
488 promoter*:mCitrine* sequences were amplified from genomic constructs described above, and
489 inserted at a *Hin*dIII site of pMpGWB301 using the In-Fusion HD Cloning System. pENTR
490 MpTUB2 was kindly provided from Dr. R. Nishihama and introduced into
491 pMpGWB301$_{pro}$Mp*SYP2:mCitrine*-GW (Fig. S2A) using the Gateway LR Clonase™ II Enzyme
492 Mix. For construction of the genome-editing vectors, the target sequences were selected using
493 CRISPR direct (https://crispr.dbcls.jp/) [39], and double-stranded oligonucleotides of the target
494 sequences were inserted into the pMpGE_En03 vector [40]. The resultant gRNA cassettes were
495 introduced into the pMpGE010 or pMpGE011 vectors [40] using the Gateway LR Clonase II
496 Enzyme Mix. For construction of the homologous recombination-mediated gene targeting vector,
497 the 3.5-kb homologous genomic sequences were amplified from the Tak-1 genome and inserted
498 at *Pac*I and *Asc*I sites of the pJHY-TMp1 vector [41] using the In-Fusion HD Cloning System.

499 Plant materials and Transformation

500 Marchantia accession Takaragaike-1 (Tak-1, male) and Takaragaike-2 (Tak-2, female) [42]
501 were used throughout the study. The growth conditions and transformation methods were
502 previously described [13,42,43]. *M. polymorpha* expressing mCitrine-MpSYP12A, mCitrine-
503 MpSYP12B, mCitrine-MpSYP13A, mCitrine-MpSYP13B, mCitrine-MpSYP2 or mCitrine-
504 MpVAMP71 under the regulation of their own regulatory elements (e.g. promoter, UTRs, and
505 introns), and *M. polymorpha* expressing mRFP-MpSYP6A or GFP-HDEL driven by the
506 Mp*EF1α* promoter were previously reported [13,38,44].
507
508 Genotyping

509 Genomic DNA was extracted from the thalli in an extraction buffer containing 1 M KCl,
510 100 mM Tris-HCl (pH 9.5), and 10 mM EDTA. This DNA was used as templates for PCR.
511 Genome fragments with putative mutation sites were amplified by PCR using KOD FX Neo
512 (TOYOBO, Osaka, Japan) according to the manufacturer's instructions. The primers used in
513 PCR-based genotyping are listed in Supplementary Table S2.
514
515 Confocal laser scanning microscopy

516 Two- and five-day-old thalli were used for imaging the cell plate and the oil body,
517 respectively. Samples were mounted in distilled water and observed using an LSM780 confocal
518 microscope (Carl Zeiss) equipped with an oil immersion lens (63×, numerical aperture = 1.4) on
519 an electrically driven stage. Gemmae were observed with a 10× objective lens (numerical
520 aperture = 0.45). Thalli were incubated in 10 μM *N*-(3-triethylammoniumpropyl)-4-(6-(4-
521 (diethylamino)phenyl)hexatrienyl) pyridinium dibromide (FM4-64, Thermo Fisher) solution for
522 2 min. Samples were then washed twice in water before observation. For 4,4-difluoro-1,3,5,7,8-
523 pentamethyl-4-bora-3a,4a-diaza-*s*-indacene (BODIPY 493/503, Thermo Fisher) staining, thalli
524 or gemmae were incubated in 200 nM BODIPY 493/503 dissolved in water for 10 min and then
525 washed twice in water before observation. The samples were excited at 488 nm (Argon 488) and
526 561 nm (DPSS 561-10) lasers, respectively, and the fluorescent emission was collected between
527 482-659 nm using twenty GaAsP detectors. Spectral unmixing and constructing maximum
528 intensity projection images were conducted using the ZEN2012 software (Carl Zeiss). Image

529 processing was performed with ZEN2012 software, Photoshop software (Adobe Systems), and
530 ImageJ (National Institute of Health, https://imagej.nih.gov/ij/).
531
532 Electron microscopy
533 Five-day-old *M. polymorpha* thalli from Tak-1 and thalli expressing mCitrine-
534 MpSYP12B were used for the immunoelectron microscopic observation. Sample preparation and
535 observation were performed as previously reported [13]. Five-day-old Tak-1 thalli were used for
536 morphological observation with a transmission electron microscope. Sample preparation and
537 observation were performed as previously reported [44].
538
539 Light sheet microscopy
540 Five-day-old thalli expressing 2×Citrine driven by the Mp*SYP12B* promoter were embedded
541 in low melt agarose gel and observed using a Light sheet Z.1 microscope (Carl Zeiss) equipped
542 with a water immersion lens (5×, numerical aperture = 0.16). The samples were excited at 488
543 nm (Argon 488 laser). Acquisition and construction of three-dimension images from multi-angle
544 images were conducted using the ZEN2014 software (Carl Zeiss). The images were processed
545 digitally with Imaris (Bitplane) and Photoshop software.
546
547 Fluorescent stereoscopic microscopy
548 Three-week-old wild-type and Mp*erf13*^{ge} thalli were stained by BODIPY493/503
549 (ThermoFisher) and observed using a fluorescent stereoscopic microscope (M165 FC, Leica)
550 equipped with a MC170 HD digital camera (Leica).
551
552 Forward genetic screening for the oil body formation mutants
553 The workflow of the mutant screening is described in Fig. S4A. Liverworts with transfer
554 DNA (T-DNA) insertions were generated by co-culture of *M. polymorpha* sporelings with the
555 agrobacteria strain GV2260 harbouring the binary vector pCAMBIA1300
556 (https://cambia.org/welcome-to-cambialabs/cambialabs-projects/cambialabs-projects-legacy-
557 pcambia-vectors-pcambia-legacy-vectors-1/cambialabs-projects-legacy-pcambia-vectors-list-of-
558 legacy-pcambia-vectors-3/). T_1 plants were first selected on 1/2× Gamborg's B5 plates
559 containing 10 mgL^{-1} hygromycin and 100 mgL^{-1} cefotaxime. Hygromycin-resistant T_1 plants

560 were then transferred and incubated on hygromycin-free medium for about one week, followed
561 by BODIPY 493/503 staining to visualize oil bodies. Visible screening for mutants defective in
562 oil body formation was performed using a fluorescent stereoscopic microscope (M165 FC,
563 Leica). To identify flanking sequences of T-DNA insertions, thermal asymmetric interlaced-PCR
564 (TAIL-PCR) was performed as described previously [42,45,46] with minor modifications using
565 crude-extracted DNA as templates. Flanking sequences were amplified using KOD FX neo DNA
566 polymerase and T-DNA-specific (TR1–3 and TL1–3 for right and left borders of T-DNA,
567 respectively) and universal adaptor (AD1–6) primers. The reaction cycles are shown below.
568 After agarose gel electrophoresis of the final TAIL-PCR products, DNA bands were excised and
569 purified using the Wizard SV Gel and PCR Clean-Up System (Promega). Purified products were
570 directly sequenced using TR3 or TL3 primers. The T-DNA insertion sites were identified using
571 the genome sequence registered in MarpolBase, genome version 3.1.
572 Cycling conditions for TAIL-PCR

573

Reaction	Cycle No.	Thermal settings
Primary	1	94°C 1 min, 95°C 1 min
	5	94°C 1 min, 65°C 1 min, 68°C 3 min
	1	94°C 1 min, 30°C 1min Ramping to 68°C 3 min, 68°C 3 min
	13	94°C 30 sec, 68°C 4 min 94°C 30 sec, 68°C 4 min 94°C 30 sec, 44°C 1 min, 68°C 3min
	1	68°C 5 min
Secondary	1	94°C 1 min, 95°C 1 min
	13	94°C 30 sec, 68°C 4 min 94°C 30 sec, 68°C 4 min 94°C 30 sec, 44°C 1 min, 68°C 3 min
	1	68°C 5 min
Tertiary	1	94°C 1 min, 95°C 1 min
	13	94°C 30 sec, 68°C 4 min 94°C 30 sec, 68°C 4 min 94°C 30 sec, 44°C 1 min, 68°C 3 min
	1	68°C 5 min

574
575
576
577
578
579
580
581
582
583
584
585
586
587
588
589
590

591 RNA extraction and RNA sequencing analysis

592 Total RNA from Tak-1, Mp*erf13*^{GOF} and Mp*erf13-1*^{ge} thalli was extracted by RNeasy
593 (QIAGEN) according to the manufacturer's instructions. The eluted total RNA samples were
594 treated with DNase I (Takara) to remove DNA contamination. The quality and quantity of the
595 total RNA were evaluated with a NanoDrop 1000 spectrophotometer (Thermo Fisher Scientific),
596 Qubit 2.0 Fluorometer (Thermo Fisher Scientific) and a Bioanalyzer RNA6000 Nano Kit
597 (Agilent Technologies). The sequence libraries were prepared with the TruSeq RNA Sample
598 Prep Kit v2 (Illumina) according to the manufacturer's low sample protocol. The quality and
599 quantity of each library were determined using a Bioanalyzer with the High Sensitivity DNA kit
600 (Agilent Technologies) and the KAPA Library Quantification Kit for Illumina (Illumina). Equal
601 amounts of each library were mixed to make the 2 nM pooled library. Illumina sequencing was
602 performed using a HiSeq 1500 platform (Illumina) to produce 126-bp single-end reads. Three
603 biological replicates were prepared for the library construction and RNA-Seq analysis. All reads
604 are available through the Sequence Read Archive (SRA) under the accession number
605 DRA009193. The abundance of transcripts from Illumina RNA-Seq data were quantified with
606 the kallisto program (version 0.43.1) [47] with the default parameters using the primary transcript
607 dataset from the Marchantia genome version 3.1. To estimate differentially expressed genes
608 (DEGs), an ANOVA-like test was performed by edgeR (version 3.18.1) [48]. Genes with FDR
609 values lower than 0.01 and an absolute $\log_2$ fold change (FC) > 2 were considered to be
610 differentially expressed. Among all combinations of DEGs ($\log_2$FC(Mp*erf13*^{GOF}/Tak-1) > 2 and
611 $\log_2$FC(Mp*erf13-1*^{ge}/Tak-1) > 2, $\log_2$FC(Mp*erf13*^{GOF}/Tak-1) > 2 and $\log_2$FC(Mp*erf13-1*^{ge}/Tak-1)
612 < -2, $\log_2$FC(Mp*erf13*^{GOF}/Tak-1) < -2 and $\log_2$FC(Mp*erf13-1*^{ge}/Tak-1) > 2,
613 $\log_2$FC(Mp*erf13*^{GOF}/Tak-1) < -2 and $\log_2$FC(Mp*erf13-1*^{ge}/Tak-1) < -2), we selected the set
614 $\log_2$FC(Mp*erf13*^{GOF}/Tak-1) > 2 and $\log_2$FC(Mp*erf13-1*^{ge}/Tak-1) < -2 as candidate genes
615 regulated downstream of MpERF13, which included both Mp*ERF13* and Mp*SYP12B*.
616

617 Quantitative reverse transcription (qRT)-PCR

618 For qRT-PCR, cDNA was synthesized from total RNA using SuperScript III Reverse
619 Transcriptase (Invitrogen) and an oligo dT(18) primer according to the manufacturer's
620 instructions. qRT-PCR was performed with LightCycler 480 (Roche) using FastStart SYBR
621 Green Master (Roche) according to the manufacturer's protocol. Sequences of primers used are

listed in Table S2. Mp*APT* (Mapoly0100s0027.1 / Mp3g25140.1) was used as a housekeeping reference for normalization [49]. Three biological replicates were prepared and three technical replicates were performed for each reaction.

Pill bug feeding assay

Feeding assay was performed according to Nakazaki *et al.* with modification [50]. Gemmae were cultured on 1/2× Gamborg's B5 medium containing 1% (w/v) agar and 1% (w/v) sucrose for five days at 22°C under continuous white light (50 μmol $m^{-2}s^{-1}$). Five-day-old thalli were transferred onto 1/2× Gamborg's B5 medium containing 1% (w/v) agar without sucrose and cultured for additional five days under the same conditions. Pill bugs (*Armadillidium vulgare*) were collected in the Myodaiji area of NIBB (Nishigonaka 38, Myodaiji, Okazaki 444-8585 Aichi, Japan). Pill bugs were maintained on Prowipe (Daio Paper, Tokyo, Japan) moistened with sterilized water for 48 h at 22°C in the dark without feeding before the assay. Six pill bugs were introduced into each medium plate containing 10-day-old thalli and kept for 24 h in the dark at 22°C. The thallus areas were calculated using ImageJ (National Institute of Health, https://imagej.nih.gov/ij/).

Gene accession numbers

Symbol	Gene ID (ver3.1)	Gene ID (ver5.1)
Mp*SYP12A*	Mapoly0163s0015	Mp6g00050
Mp*SYP12B*	Mapoly0101s0013	Mp4g20670
Mp*SYP13A*	Mapoly0009s0005	Mp7g13190
Mp*SYP13B*	Mapoly0055s0091	Mp2g19600
Mp*CLC1*	Mapoly0075s0069	Mp2g03080
Mp*PIP2*	Mapoly0041s0003	Mp4g17210
Mp*ERF13*	Mapoly0060s0052	Mp6g08690
Mp*ABCG1*	Mapoly0083s0014	Mp8g13070
Mp*MYB02*	Mapoly0006s0226	Mp3g07510
Mp*TUB2*	Mapoly0158s0010 [51,52]	Mp2g09390
Mp*SYP6A*	Mapoly0140s0004	Mp3g18380
Mp*SYP2*	Mapoly0187s0013	Mp8g15260
Mp*SFT1*	Mapoly0006s0109	Mp3g06390
Mp*GOS11*	Mapoly0001s0245	Mp1g19070
Mp*SYP4*	Mapoly0042s0041	Mp2g14140
Mp*VAMP71*	Mapoly0064s0109	Mp8g00880
Mp*SEC20*	Mapoly0019s0137	Mp1g13670

Mp*USE1A*	Mapoly0001s0213	Mp1g18750
Mp*SEC22*	Mapoly0023s0071	Mp2g11050
Mp*CYCB1*	Mapoly0048s0068	Mp5g10030

640

641 We followed the nomenclature of genes, proteins, and mutants of Marchantia reported in
642 Bowman *et al*. (2016) [53]. Gene IDs were taken from MarpolBase (http://marchantia.info/),
643 genome version 3.1 and version 5.1 [20,54].
644

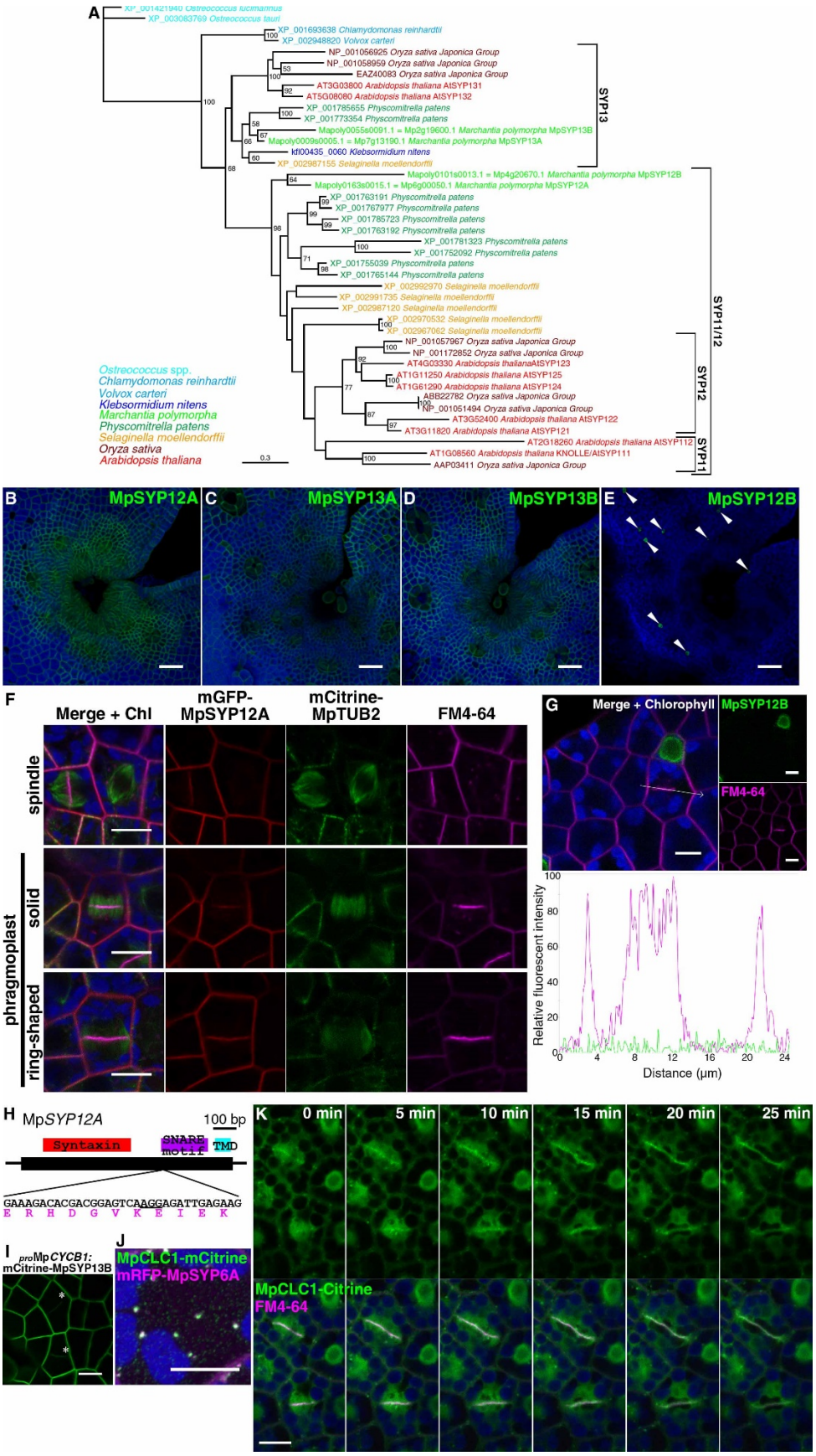

Fig. S1. Characterization of SYP1 member and clathrin light chain localization during

646 **cytokinesis in Marchantia thalli**

647 (A) A maximum likelihood phylogenetic tree of SYP1 members in green plants. Although the
648 tree is unrooted, the proteins from Chlorophytes (*Ostreococcus* spp., *Chlamydomonas*
649 *reinhardtii*, and *Volvox carteri*) are the outgroup to those of streptophytes. The branch lengths
650 are proportional to the estimated number of substitutions per site. Bootstrap probability is
651 indicated as a percentage on each branch with at least 50% support. (B - E) Maximum intensity
652 projection images of thalli expressing mCitrine-MpSYP12A (B), mCitrine-MpSYP13A (C),
653 mCitrine-MpSYP13B (D), or mCitrine-MpSYP12B (E). White arrowheads indicate mCitrine-
654 MpSYP12B-expressing cells. (F) Single confocal images of thallus cells expressing mCitrine-
655 MpTUB2 and mGFP-MpSYP12A under the regulation of the Mp*SYP2* and Mp*SYP12A*
656 promoters, respectively, stained with FM-4-64. In mitotic cells, spindles and phragmoplasts
657 (solid and ring-shaped phases) were labelled by mCitrine-MpTUB2, and endocytosed FM-4-64
658 accumulated at forming cell plates. (G) Single confocal images of thallus cells expressing
659 mCitrine-MpSYP12B stained with FM4-64. The line graph indicates the relative fluorescence
660 intensity along the white arrow. Relative fluorescent intensity of mCitrine to fluorescence on the
661 oil body membrane is shown for mCitrine fluorescence. (H) The gene model and sequences of
662 MpSYP12A. The syntaxin domain, SNARE motif, and transmembrane domain (TMD) are
663 shown above the gene model. Black and magenta letters indicate genome and translated amino
664 acid sequences. The protospacer adjacent motif (PAM) sequence for gRNA is underlined. (I)
665 Expression by the Mp*CYCB1* promoter results in accumulation of MpSYP13B at the forming
666 cell plate. A single confocal image of dividing thallus cells expressing mCitrine-MpSYP13B are
667 shown. Asterisks indicate forming cell plates. (J) A maximum intensity projection image of a
668 thallus cell expressing MpCLC1-mCitrine and mRFP-MpSYP6A under the regulation of their
669 own regulatory elements and the Mp*EF1α* promoter, respectively. (K) Time-lapse single
670 confocal images of thallus cells expressing MpCLC1-Citrine under the regulation of the
671 Mp*EF1α* promoter (upper panels) and merged images with FM4-64 signals. Autofluorescence
672 from chlorophyll is pseudo-colored in blue. Bars = 50 μm in (B - E) and 10 μm in (F), (G), (I),
673 (J), and (K).
674

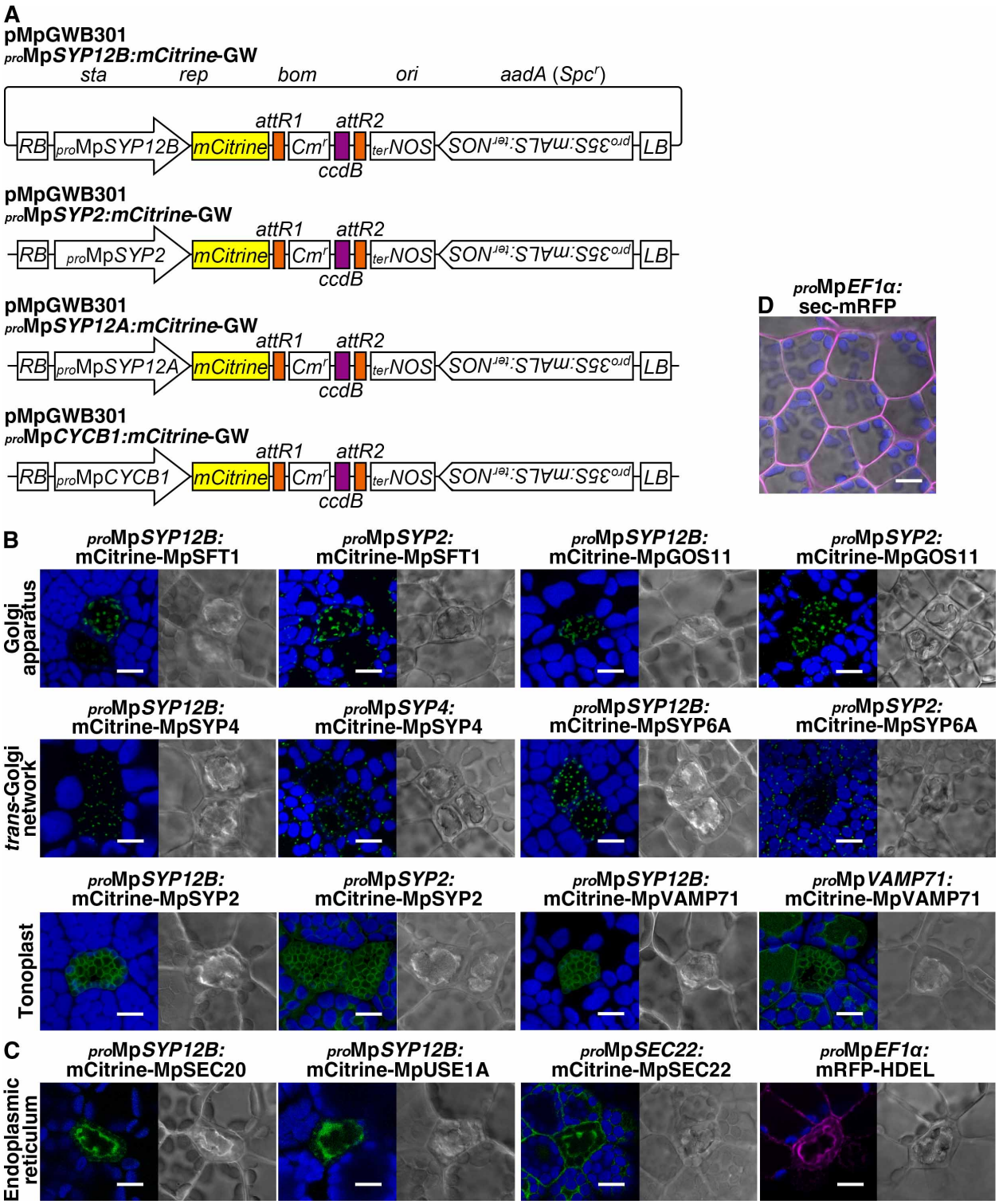

Fig. S2. Subcellular localization of organelle markers in oil body cells

(A) Gateway constructs used in this study. pMpGWB301 *pro*Mp*SYP2:*mCitrine-GW was previously prepared[44]. (B) Maximum intensity projection images of thallus cells including the oil

678 body cell expressing mCitrine-fused markers for the Golgi apparatus (MpSFT1 and MpGOS11),
679 *trans*-Golgi network (MpSYP4 and MpSYP6A), and tonoplast (MpSYP2 and MpVAMP71).
680 The organelle markers were expressed under the Mp*SYP12B*, Mp*SYP2*, and/or own promoters.
681 Bright field images are also shown. (C) Single confocal images of thallus cells including the oil
682 body cell expressing endoplasmic reticulum markers. mCitrine-MpSEC20 and mCitrine-
683 MpUSE1A were expressed under the Mp*SYP12B* promoter. mCitrine-MpSEC22 and mRFP-
684 HDEL were expressed using their own regulatory elements and the Mp*EF1α* promoter,
685 respectively. (D) A single confocal image of thallus cells expressing sec-mRFP expressed under
686 the Mp*EF1α* promoter. Green, magenta, and blue pseudo-colors indicate fluorescence from
687 mCitrine, mRFP, and chlorophyll, respectively. Bars = 10 μm.
688

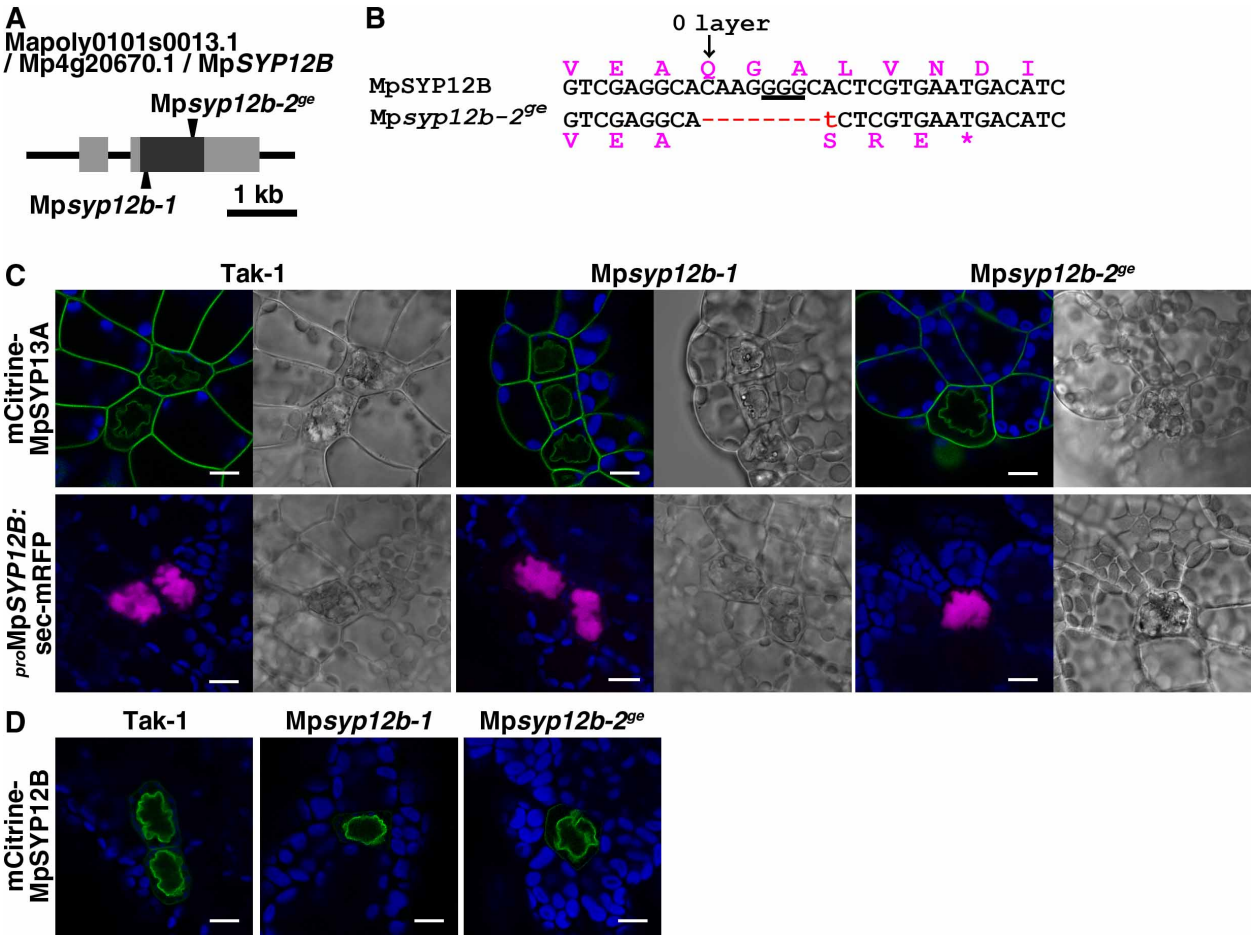

Fig. S3. Phenotype of Mp*syp12b* mutants

(A) Schematic representation of the Mp*SYP12B* gene structure. Gray and black boxes indicate untranslated and coding regions, respectively, and arrowheads indicate mutation sites in two independently generated mutants. The Mp*syp12b-1* mutant was generated by a homologous recombination-mediated gene targeting method[41]. (B) The genome (black letters) and translated amino acid (magenta letters) sequences of Mp*SYP12B* and the Mp*syp12b-2*^{ge} mutant, with the red letters indicating the mutated region. The PAM sequence for gRNA is underlined. The 0 layer at the centre of the SNARE motif is shown. (C) Single confocal images of thallus cells including the oil body cell expressing mCitrine-MpSYP13A under its own regulatory elements, or sec-mRFP under the Mp*SYP12B* promoter in Tak-1, Mp*syp12b-1*, and Mp*syp12b-2*^{ge} lines. Bright field images are also shown. (D) Single confocal images of thallus cells including the oil body cell expressing mCitrine-MpSYP12B under its own regulatory elements in Tak-1 and Mp*syp12b* mutants. Green, magenta, and blue pseudo-colors indicate fluorescence from mCitrine, mRFP, and chlorophyll, respectively. Bars = 10 μm.

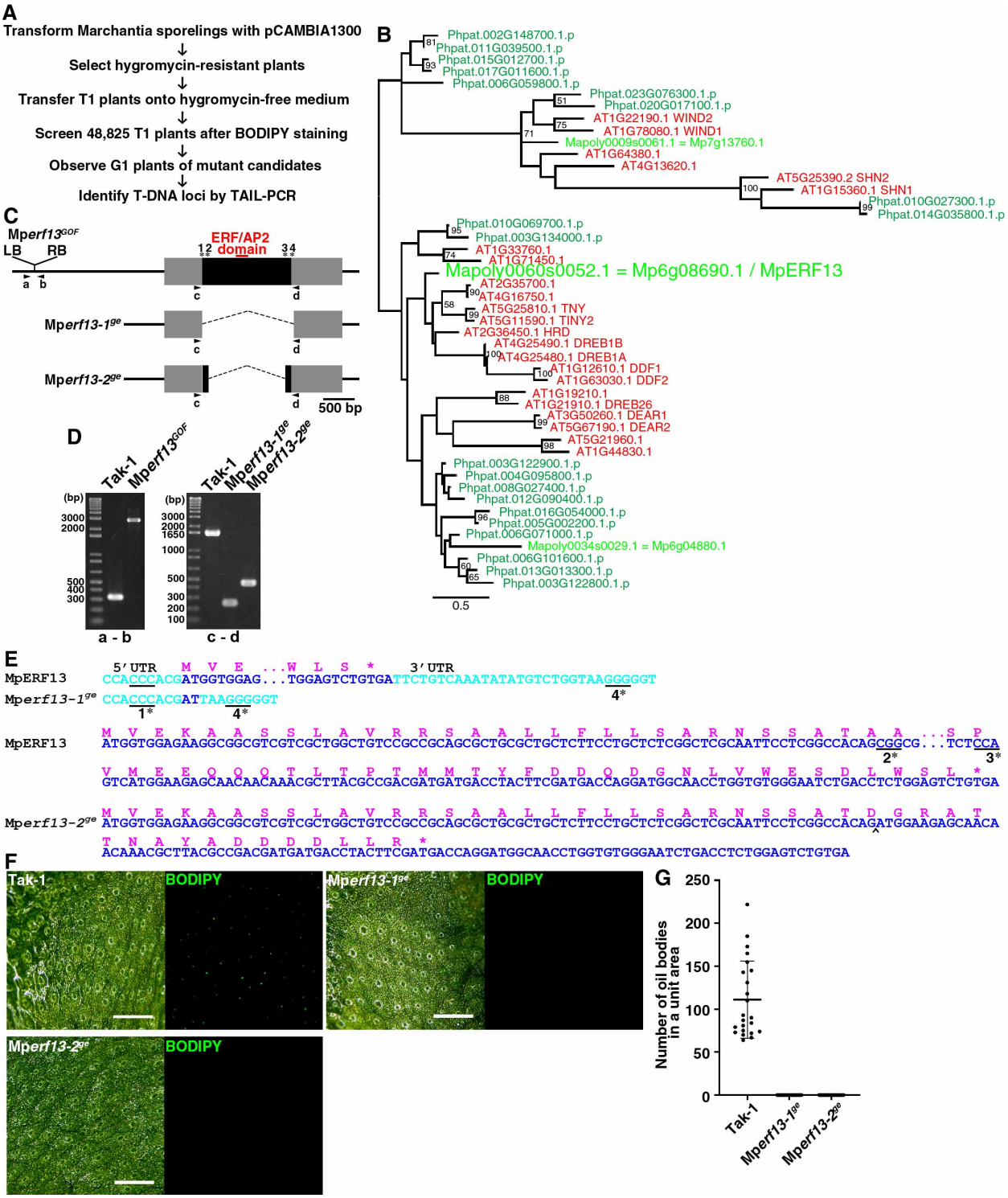

Fig. S4. Screening and generation of Mp*erf13* mutants

(A) The flow chart of the screen for mutants defective in oil body formation from T-DNA-insertion lines. (B) A maximum likelihood phylogenetic tree of proteins with one ERF/AP2 domain. The color code is shown in Fig S1A. The branch lengths are proportional to the

707 estimated number of substitutions per site. Bootstrap probability is indicated as a percentage on
708 each branch with at least 50% support. A more detailed tree was presented previously (*20*). (C)
709 Schematic representation of the Mp*ERF13* gene structure and mutations generated in this study.
710 Gray and black boxes indicate the UTR and coding sequences, respectively. Asterisks with
711 numbers indicate sites of designed gRNA to generate Mp*erf13-1*^{ge} (*1 and *4) and Mp*erf13-2*^{ge}
712 (*2 and *3). (D) PCR-based genotyping of Tak-1, Mp*erf13*^{GOF}, Mp*erf13-1*^{ge}, and Mp*erf13-2*^{ge}.
713 The combinations and annealing sites of primers (a to d) are shown in (C). (E) The genomic and
714 predicted amino acid sequences of the Mp*ERF13* locus in Tak-1 and Mp*erf13* mutants. Light
715 blue, dark blue, and magenta letters indicate UTR, coding, and predicted amino acid sequences,
716 respectively. The PAM sequences for gRNAs are underlined. The caret indicates the indel site.
717 (F) Fluorescent and bright-field images of BODIPY-stained three-week-old thalli of Tak-1,
718 Mp*erf13-1*^{ge}, and Mp*erf13-2*^{ge}. Bars = 0.5 mm. (G) The number of oil bodies visualized with
719 BODIPY in a unit area (2.0 mm × 2.0 mm). Bars indicate means ± SD. Statistical analyses
720 between Tak-1 and each genotype were conducted using a two-tailed Welch's *t*-test. Sample
721 numbers were 23 thalli for Tak-1, 24 for Mp*erf13-1*^{ge}, and 26 for Mp*erf13-2*^{ge}. *p*-values are
722 5.14×10^{-11} for Mp*erf13-1*^{ge} and 5.14×10^{-11} for Mp*erf13-2*^{ge}.
723

A

Gene ID Ver3.1	Gene ID Ver5.1	Description	logFC (Mp*erf13*^{GOF}/Tak-1)	logFC (Mp*erf13-1*^{ge}/Tak-1)
Mapoly0083s0014	Mp8g13070	ABC transporter	4.273	-3.722
Mapoly2351s0001	Mp2g20510	Cytochrome P450	6.795	-5.717
Mapoly0119s0008	Mp4g14860	LEA protein	5.045	-3.099
Mapoly0101s0013	Mp4g20670	MpSYP12B	4.374	-5.777
Mapoly0006s0226	Mp3g07510	MpMYB02	3.053	-7.208
Mapoly0060s0052	Mp6g08690	MpERF13	4.734	-5.205
Mapoly0110s0019	Mp8g13380	Cellulase	4.005	-6.537
Mapoly0005s0135	Mp1g04730	Lipid transfer	4.454	-4.903
Mapoly0081s0021	Mp8g05200	Receptor-like kinase	2.813	-4.406
Mapoly0060s0009	Mp6g09100	Ankyrin repeats	4.243	-5.086
Mapoly0207s0009	Mp2g24710	Tomosyn12	3.698	-5.704

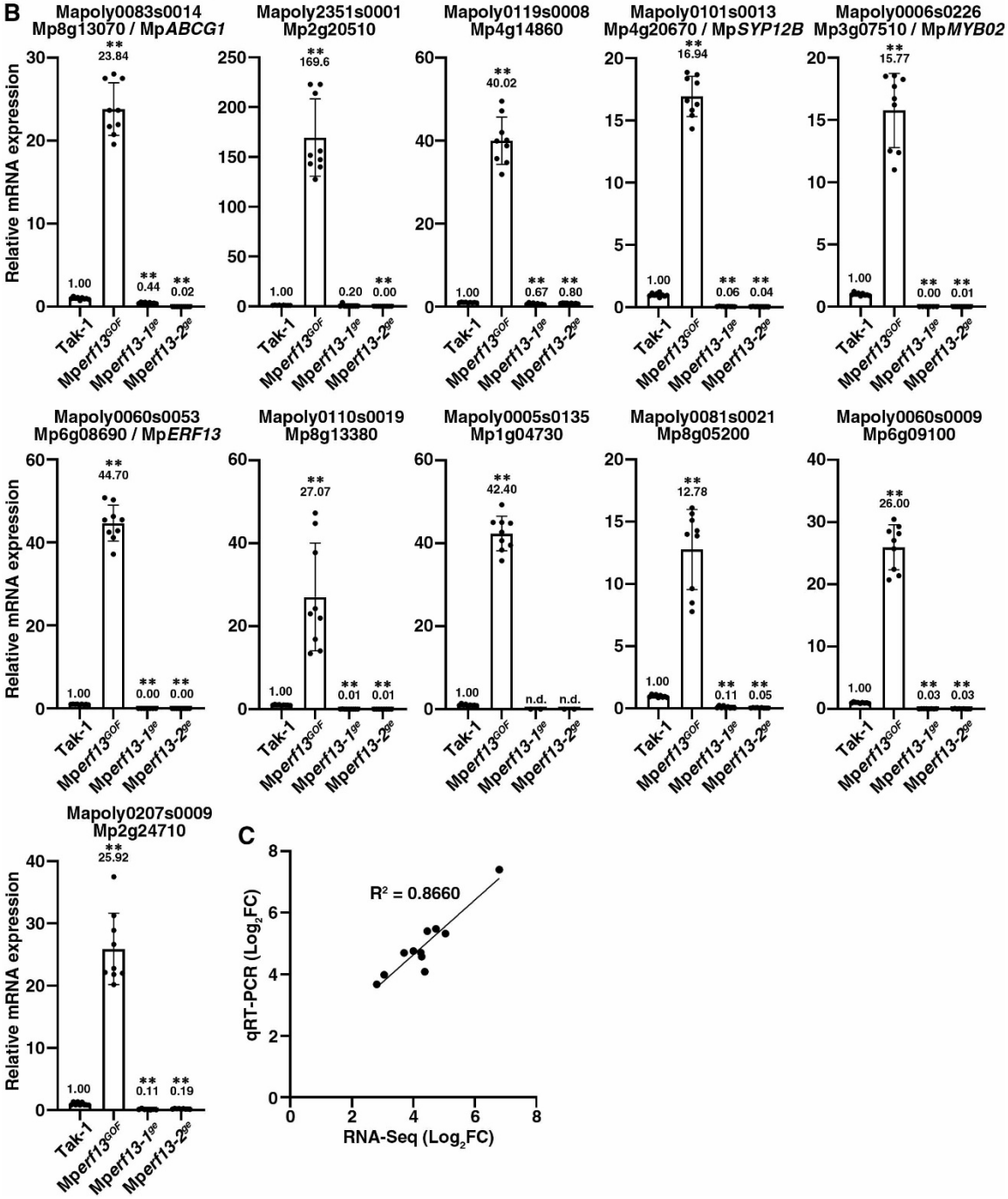

724 **Fig. S5. Gene expression in Mp*erf13* mutants**

725 (A) List of selected differentially expressed genes (DEGs) for qRT-PCR analysis. The full list of
726 DEGs are shown as Supplementary Table S1. (B) The relative mRNA expression of 11 DEGs in
727 Tak-1, Mp*erf13*^{GOF}, Mp*erf13-1*^{ge}, and Mp*erf13-2*^{ge} measured by qRT-PCR. Mp*APT* was used as
728 an internal reference. Error bars represent ± SD. Means are indicated above the bars. Statistical
729 comparison between Tak-1 and each genotype was conducted with a two-tailed Welch's *t*-test.
730 **, $p < 0.01$. (C) Correlation of the expression levels between the RNA-Seq analysis and qRT-
731 PCR experiment. Both the x- and y- axes are shown in a $\log_2$FC scale. R^2 indicates the
732 correlation coefficient.
733

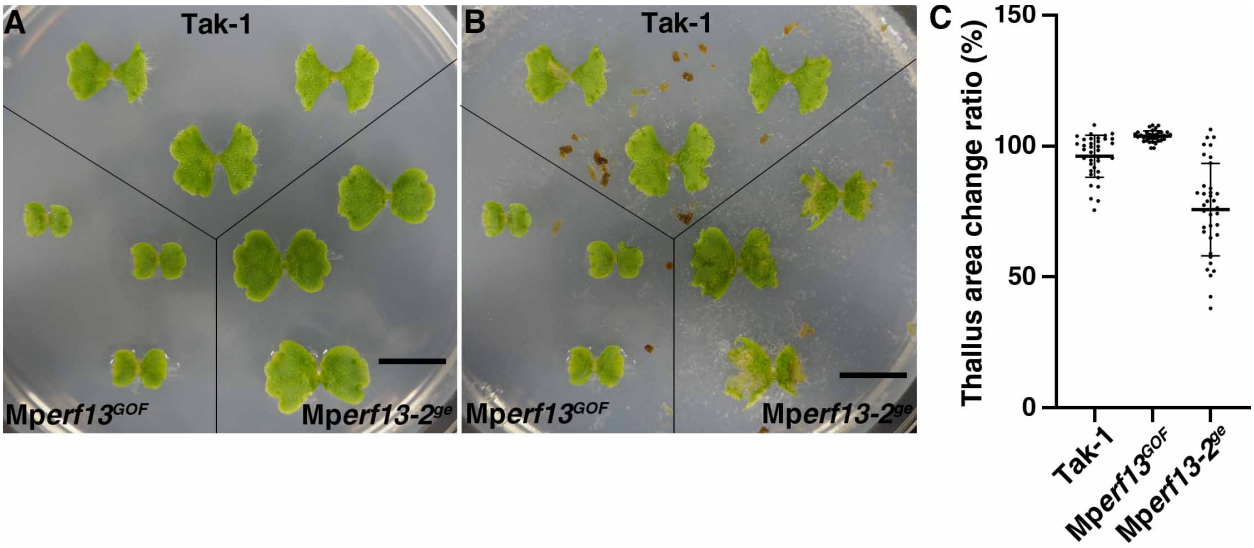

Fig. S6. Pill bug feeding assay

(A and B) Ten-day-old thalli of Tak-1, Mp*erf13*^{GOF} and Mp*erf13-2*^{ge} (A) were co-cultivated with starved pill bugs for 24 hr (B). Bars = 1 cm. (C) Ratios of thallus area before and after co-cultivation with pill bugs were calculated (n = 36 thalli for each genotype). Bars indicate means ± SD. Statistical analyses between Tak-1 and each genotype were conducted with a two-tailed Welch's *t*-test. The *p*-values were 1.63×10^{-5} for Mp*erf13*^{GOF} and 4.91×10^{-6} for Mp*erf13-2*^{ge}.

741 **Table S1.** The list of DEGs in Mp*erf13* mutants identified in RNA-Seq analysis.

742 **Table S2.** List of primers used in this study.

743

744 **Movie S1. Formation of clathrin-coated vesicles at the oil body membrane**.

745 A time-lapse movie of an oil body cell expressing MpCLC1-Citrine. Green and blue pseudo-
746 colors represent fluorescence from Citrine and chlorophyll, respectively. 32× real time. Bar = 5
747 μm.

748 **Movie S2. Expression of MpSYP12B in a Marchantia thallus**

749 A five-day-old thallus expressing 2×YFP driven by the Mp*SYP12B* promoter observed by light
750 sheet microscopy. Green and blue pseudo-colors represent fluorescence from Citrine and
751 chlorophyll, respectively. Bar = 400 μm.

752

753

754 **References:**

755 33 Edgar, R. C. MUSCLE: a multiple sequence alignment method with reduced time and
756 space complexity. *BMC bioinformatics* **5**, 113, doi:10.1186/1471-2105-5-113 (2004).

757 34 Edgar, R. C. MUSCLE: multiple sequence alignment with high accuracy and high
758 throughput. *Nucleic acids research* **32**, 1792-1797, doi:10.1093/nar/gkh340 (2004).

759 35 Castresana, J. Selection of conserved blocks from multiple alignments for their use in
760 phylogenetic analysis. *Mol Biol Evol* **17**, 540-552, doi:DOI
761 10.1093/oxfordjournals.molbev.a026334 (2000).

762 36 Talavera, G. & Castresana, J. Improvement of phylogenies after removing divergent and
763 ambiguously aligned blocks from protein sequence alignments. *Syst Biol* **56**, 564-577,
764 doi:10.1080/10635150701472164 (2007).

765 37 Guindon, S. *et al.* New Algorithms and Methods to Estimate Maximum-Likelihood
766 Phylogenies: Assessing the Performance of PhyML 3.0. *Syst Biol* **59**, 307-321,
767 doi:10.1093/sysbio/syq010 (2010).
768 38 Ishizaki, K. *et al.* Development of Gateway Binary Vector Series with Four Different
769 Selection Markers for the Liverwort *Marchantia polymorpha*. *PloS one* **10**, e0138876,
770 doi:10.1371/journal.pone.0138876 (2015).
771 39 Naito, Y., Hino, K., Bono, H. & Ui-Tei, K. CRISPRdirect: software for designing
772 CRISPR/Cas guide RNA with reduced off-target sites. *Bioinformatics* **31**, 1120-1123,
773 doi:10.1093/bioinformatics/btu743 (2015).
774 40 Sugano, S. S. *et al.* Efficient CRISPR/Cas9-based genome editing and its application to
775 conditional genetic analysis in *Marchantia polymorpha*. *PloS one* **13**, e0205117,
776 doi:10.1371/journal.pone.0205117 (2018).
777 41 Ishizaki, K., Johzuka-Hisatomi, Y., Ishida, S., Iida, S. & Kohchi, T. Homologous
778 recombination-mediated gene targeting in the liverwort *Marchantia polymorpha* L.
779 *Scientific reports* **3**, 1532, doi:10.1038/srep01532 (2013).
780 42 Ishizaki, K., Chiyoda, S., Yamato, K. T. & Kohchi, T. Agrobacterium-mediated
781 transformation of the haploid liverwort *Marchantia polymorpha* L., an emerging model
782 for plant biology. *Plant & cell physiology* **49**, 1084-1091, doi:10.1093/pcp/pcn085
783 (2008).
784 43 Kubota, A., Ishizaki, K., Hosaka, M. & Kohchi, T. Efficient Agrobacterium-mediated
785 transformation of the liverwort *Marchantia polymorpha* using regenerating thalli.
786 *Bioscience, biotechnology, and biochemistry* **77**, 167-172, doi:10.1271/bbb.120700
787 (2013).

788 44 Minamino, N. *et al.* Dynamic reorganization of the endomembrane system during
789 spermatogenesis in *Marchantia polymorpha*. *Journal of plant research* **130**, 433-441,
790 doi:10.1007/s10265-017-0909-5 (2017).
791 45 Honkanen, S. *et al.* The Mechanism Forming the Cell Surface of Tip-Growing Rooting
792 Cells Is Conserved among Land Plants. *Curr Biol* **26**, 3238-3244,
793 doi:10.1016/j.cub.2016.09.062 (2016).
794 46 Liu, Y. G., Mitsukawa, N., Oosumi, T. & Whittier, R. F. Efficient Isolation and Mapping
795 of *Arabidopsis-thaliana* T-DNA Insert Junctions by Thermal Asymmetric Interlaced Pcr.
796 *Plant Journal* **8**, 457-463, doi:DOI 10.1046/j.1365-313X.1995.08030457.x (1995).
797 47 Bray, N. L., Pimentel, H., Melsted, P. & Pachter, L. Near-optimal probabilistic RNA-seq
798 quantification. *Nature biotechnology* **34**, 525-527, doi:10.1038/nbt.3519 (2016).
799 48 Robinson, M. D., McCarthy, D. J. & Smyth, G. K. edgeR: a Bioconductor package for
800 differential expression analysis of digital gene expression data. *Bioinformatics* **26**, 139-
801 140, doi:10.1093/bioinformatics/btp616 (2010).
802 49 Saint-Marcoux, D., Proust, H., Dolan, L. & Langdale, J. A. Identification of reference
803 genes for real-time quantitative PCR experiments in the liverwort *Marchantia*
804 *polymorpha*. *PloS one* **10**, e0118678, doi:10.1371/journal.pone.0118678 (2015).
805 50 Nakazaki, A. *et al.* Leaf Endoplasmic Reticulum Bodies Identified in Arabidopsis Rosette
806 Leaves Are Involved in Defense against Herbivory. *Plant physiology* **179**, 1515-1524,
807 doi:10.1104/pp.18.00984 (2019).
808 51 Buschmann, H., Holtmannspotter, M., Borchers, A., O'Donoghue, M. T. & Zachgo, S.
809 Microtubule dynamics of the centrosome-like polar organizers from the basal land plant

810 *Marchantia polymorpha*. *The New phytologist* **209**, 999-1013, doi:10.1111/nph.13691
811 (2016).
812 52 Otani, K. *et al.* An evolutionarily conserved NIMA-related kinase directs rhizoid tip
813 growth in the basal land plant *Marchantia polymorpha*. *Development* **145**,
814 doi:10.1242/dev.154617 (2018).
815 53 Bowman, J. L. *et al.* The Naming of Names: Guidelines for Gene Nomenclature in
816 Marchantia. *Plant & cell physiology* **57**, 257-261, doi:10.1093/pcp/pcv193 (2016).
817 54 Montgomery, S. A. *et al.* Chromatin Organization in Early Land Plants Reveals an
818 Ancestral Association between H3K27me3, Transposons, and Constitutive
819 Heterochromatin. *Curr Biol*, doi:10.1016/j.cub.2019.12.015 (2020).